Journal of Thermal Analysis and Calorimetry (2023) 148:14051–14068
https://doi.org/10.1007/s10973-023-12594-3

Experimental investigation and performance optimization of thermo-hydraulic and exergetic characteristics of a novel multi-fluid heat exchanger

Belal Almasri[1] · **Taraprasad Mohapatra**[1] · **Sudhansu S. Mishra**[2]

Received: 27 March 2023 / Accepted: 16 September 2023 / Published online: 21 November 2023

Abstract
In this research, the thermo-hydraulic performance of a multi-fluid heat exchanger is experimentally investigated in regard to variations in control parameters, namely flow rate, flow configuration, and inlet temperature. A brazed helix tube (BHT), constructed from a helical coil tube with precision brazing between successive coil turns, is novel and integrated inside the present novel multi-fluid heat exchanger (NMFHE). The NMFHE presented here is part of a residential heating system where concurrent heating of cold water (HF_2) and cold air (HF_3) takes place with effective heat transfer from hot water (HF_1) flowing inside the BHT. The JF factor and entropy generation number (Ns) are considered the key performance parameters of the study and experimentally predicted with respect to variations in control factors. The HF_1 flow rate, HF_2 flow rate, and flow configuration are identified as the most effective parameters for the JF factor (HF_1, HF_2, and HF_3) with a contribution of 58.67%, 65.88%, and 34.85%, respectively. The HF_1 inlet temperature and flow configuration are identified as the most effective parameters for the Ns (HF_1, HF_2, and HF_3) with a contribution of 31.51%, 84.95%, and 98.44%, respectively. Afterward, the thermo-hydraulic performance of the NMFHE is optimized using the Taguchi–Grey technique for maximum JF factor and minimum Ns. The optimized performance of the NMFHE is predicted in counter-flow (cold water reversal) configuration with HF_1 and HF_2 flow rate of 150 LPH, and HF_1 inlet temperature of 353 K and confirmed with significant improvement in Grey relational grade of 8.36%.

Keywords Multi-fluid heat exchanger · Brazed helical tube · Thermo-hydraulic behaviour · Optimization · Taguchi–Grey technique

Abbreviations

CF1	Counter flow (hot water reverse)
CF2	Counter flow (cold water reverse)
CF3	Counter flow (cold air reverse)
HF_1	Hot water
HF_2	Cold water
HF_3	Cold air
LPH	Litre per hour
NTU	Numbers of transfer unit
PF	Parallel flow
S/N	Signal-to-noise
TFHE	Three-fluid heat exchanger
TTHE	Triple tube heat exchanger

List of symbols

D_c	Coil diameter, m
$d_{c,i}$	Helical tube diameter, m
f	Friction factor
k	Thermal conductivity, W m^{-1} K^{-1}
$\dot{m}$	Mass flow rate, kg s^{-1}
Ns	Entropy generation number
Pr	Prandtl number
q'	Heat transfer per unit length, W m^{-1}
Re	Reynolds number
T	Temperature, K

✉ Taraprasad Mohapatra
taraprasad1980@gmail.com

Belal Almasri
eng.belal.almasri@gmail.com

Sudhansu S. Mishra
sudhansumishrabls@gmail.com

1 Department of Mechanical Engineering, C. V. Raman Global University, Bhubaneswar 752054, India

2 Department of Mechanical Engineering, Government College of Engineering, Keonjhar 758002, India

Greek symbols

μh Dynamic viscosity, kg m^{-1} s^{-1}

ρ Density, Kg m^{-3}

Introduction

In many engineering fields, including power generation, chemical processing, the food industry, automotive cooling, HVAC systems, and waste heat recovery, heat exchangers are essential components. To enhance the performances of heat exchangers, several techniques have been used, mainly passive and active methods. Using design changes such as helical coils insertion, the introduction of corrugated or wavy tubes, extended fins, the introduction of nanofluids, etc., are examples of passive methods, where no energy source is used unlikely active methods. In this work, one such passive technique, i.e. brazed helix tube (BHT), is introduced in the inner core portion of the present heat exchanger for performance enhancement and differentiate from others in regard to stated novelty BHT. The BHT integration inside an outer shell converts a double-pipe heat exchanger to a novel multi-fluid heat exchanger (NMFHE), which is presently investigated experimentally to measure thermo-hydraulic and exergetic performance. For the stated performance measures, the following literature is reviewed to acknowledge a better clarity of research in this field.

Three fluid heat exchangers (TFHE) come under multi-fluid heat exchangers (MFHE) and are widely used in specific areas such as cryogenics and various chemical processes. These include systems for separating air, processing helium and hydrogen, and making ammonia gas [1]. One specific design, the triple concentric tube, is popular in the food and pharmaceutical industries. It is mainly used to heat-treat liquids such as milk and fruit juices [2]. There has been a lot of research on these three fluid heat exchangers. Studies have observed their designs, their working principles, and methods of heat transfer. A three-fluid heat exchanger with two thermal communications between the thermally imbalanced fluid streams was given a compact solution for the temperature distribution and temperature cross. There are four different fluid flow configurations that may have been examined [3]. An investigation has been done on analytical relationships between the design variables (the NTU-effectiveness relationships) for a general three-fluid heat exchanger, in which all three streams are in thermal communication [4]. In another work, nonlinear problems and the thermal design theory of multi-fluid heat exchangers (containing more than three fluid streams) and multi-stream plate-fin heat exchangers were not taken into consideration [5]. Based on the conservation of energy principle, the dimensionless governing equations for three fluid heat exchangers are constructed, and they are then resolved using FEM based on the subdomain collocation method and Galerkin's approach. As can be seen, when the obtained findings are contrasted with the analytical results for the traditional two fluid heat exchangers, the results demonstrate that the subdomain collocation approach is more accurate than Galerkin's method [6]. The effectiveness-NTU relations were derived in the study as a crucial component of the compressive theoretical investigation carried out by TTHE, and some representatives were shown in graphical form [7]. Counter-flow triple concentric-tube heat exchangers were the subject of a two-part theoretical study. The performance calculations and design calculations included in the case studies were used to show that the three tubes' relative diameters to one another are the most crucial factors affecting the exchanger's performance (or size) [8]. Theoretical investigation into TTHE includes the derivation of the governing differential equations and potential solutions under certain circumstances. The work's generated equations can be applied to both performance and design calculations, in addition to helping to estimate bulk temperature fluctuations along the exchanger [9]. A dairy triple tube heat exchanger's performance degrades when milk fouling builds up on the heating surface. A simulation model for the precise estimates of milk outflow temperature and fouling thickness. In the study that is being done, the local fouling factor is expressed in terms of the Biot number. It is possible to anticipate the fouling thickness and milk outflow temperature as a function of time and along the full heat exchanger's length [10, 11]. For the examination of multiple stream heat exchangers, a very effective algorithm has been developed. A stack of (n–1) two stream exchangers divided by diabatic partitions is thought of as an n-stream heat exchanger using this method. The full heat exchanger can be developed non-iteratively starting with the analysis of the fundamental two stream units [12]. With the aid of FEM, the performance of a triple concentric pipe heat exchanger is numerically investigated under steady-state settings for various flow configurations and for insulated as well as non-insulated heat exchanger conditions. Hot water, cold water, and regular tap water are the three fluids being taken into consideration [13]. The heat transfer and fluid flow characteristics of two different hybrid nanofluids are numerically investigated in a helical double-pipe heat exchanger with a curved conical turbulator in a laminar regime using the Fluent software [14]. An off-grid solar poly-generation system is analysed [15] in regard to energy efficiency, exergy efficiency, and economy, and found feasible. The performance of a triple concentric pipe heat exchanger was experimentally investigated under steady-state settings using identical working fluids for two distinct flow arrangements, referred to as N–H–C and C–H–N, and for insulated as well as non-insulated heat exchanger conditions. Normal water flows via the innermost pipe in the N–H–C configuration, hot water flows through the inner annulus, and cold water flows through the outer annulus [16].

Research in the field of triple concentric-tube heat exchangers (TTHE) has led to the introduction of a mathematical model tailored specifically for heat transfer analysis [17]. Notably, the potential of a wood-based home heating system was explored, with emphasis on its temperature outputs and efficiency in heat recovery [18]. Thermo-hydraulic inquiries on the TTHE with two thermal communications were conducted in a steady-state condition [19]. Both experimental and computational analyses of the TTHE accentuated the double-tube heat exchanger specifically [20]. Further, the TTHE equipped with inserted ribs received both experimental and computational analyses [21]. Volume flow rate changes were investigated to determine their impact on TFHE efficiency. As fluid flow rates increased in the TFHE, a corresponding increase in the overall heat transfer coefficient was seen, and efficiencies displayed different behaviours based on combined capacity ratios, *R*, and NTU [22]. One creative model that used Fortran provided a thorough examination of the TTHE parameters and included gases such as hydrogen, nitrogen, and oxygen [23]. Modern climate control solutions are made possible by the development of an advanced air-conditioning system that can regulate temperature and humidity simultaneously using a TFHE [24]. A spiral tube TFHE infused with various concentrations of graphene/water was specifically studied, with a focus on metrics like heat transfer efficiency [25]. A three-fluid exchanger designed for domestic heating purposes was the subject of another interesting investigation [26]. The limitation of typical air conditioners to change both temperature and humidity at once has been a persistent problem in the sector [27]. A popular three-fluid heat exchanger is the TriCoil system. It can save up to 15.8% on energy, making it an economical option for household settings. Even more impressive, little changes to its design can greatly improve its effectiveness [28].

After a detailed study on multi-fluid heat exchanger, it is concluded that the present work on multi-fluid heat exchanger with brazed helix tube proposed for enhanced performance is novel, and no information about such heat exchanger is available in the literature. Therefore, an extensive experimental study is conducted presently on NMFHE to predict its thermo-hydraulic and exergetic performance in regard to variations in flow rates, flow configurations, and inlet temperatures. Taguchi–Grey optimization technique is used to predict optimal value of input operating parameters for the optimum performance of the NMFHE, i.e. maximum JF factor and minimum entropy generation number. A confirmation test has been carried out to compare the predicted results with the experimental one and validated. Subsequent sections cover detailed analysis, optimization study, and confirmation test.

Materials and methods

Experimental investigation

Experimental setup

The present research conducts a thorough analysis of a novel multi-fluid heat exchanger (NMFHE), which is an advanced version of a traditional double-tube heat exchanger. The experimental setup of NMFHE is shown in Fig. 1.

In this design, a copper-made brazed helix tube (BHT) replaces the core inner tube in the double-tube heat exchanger. The unique structure of the BHT enables two separate flow paths; one designated for hot water (denoted as HF_1) and the other for air (referred to as HF_3). The geometrical arrangement of the BHT permits HF_3 to flow through the hollow conduit section, as shown in Fig. 2, while HF_1 circulates through the conduit, specifically between the helical tube inlet and outlet.

The cold fluid (HF_2) flows through the outer annular shell, which is the space defined between the exterior PVC tube and the BHT in Fig. 2. The NMFHE setup is a total length of 0.871 m, with a PVC outermost shell having an internal diameter of 134 mm and a wall thickness of 9.2 mm. The interior BHT is of 31.62 m in length, 6.3 mm in diameter, 0.81 mm in thickness, a pitch of 7.92 mm, a coil radius of 96.8 mm, and with 104 turns.

For the hydraulic circuit of HF_1, a centrifugal pump is fitted for the flow through the BHT. The temperature of HF_1 is increased by an electric heater, which is controlled by a thermostat for temperature control. An axial fan of diameter 4 inches supplies HF_3 at three different speeds through the hollow conduit of the inner BHT. Furthermore, using K-type thermocouples, those are positioned at four different positions throughout the NMFHE, the temperature gradients of HF_1, HF_2, and HF_3 are accurately obtained at the inlet, intermediate, and outlet stages. For adjusting the flow rates of HF_1 and HF_2, additional equipment such flow control valves and rotameters is used, for a thorough and controlled analysis of thermo-hydraulic behaviour of the system.

Experimental procedure

This study closely examines the heat transfer characteristics of the novel multi-fluid heat exchanger (NMFHE). In this investigation, the thermo-hydraulic behaviour is tested at different flow rates, varying input temperatures, and at different flow configurations. The experimental investigation comprises of three different volume flow rates of HF_1

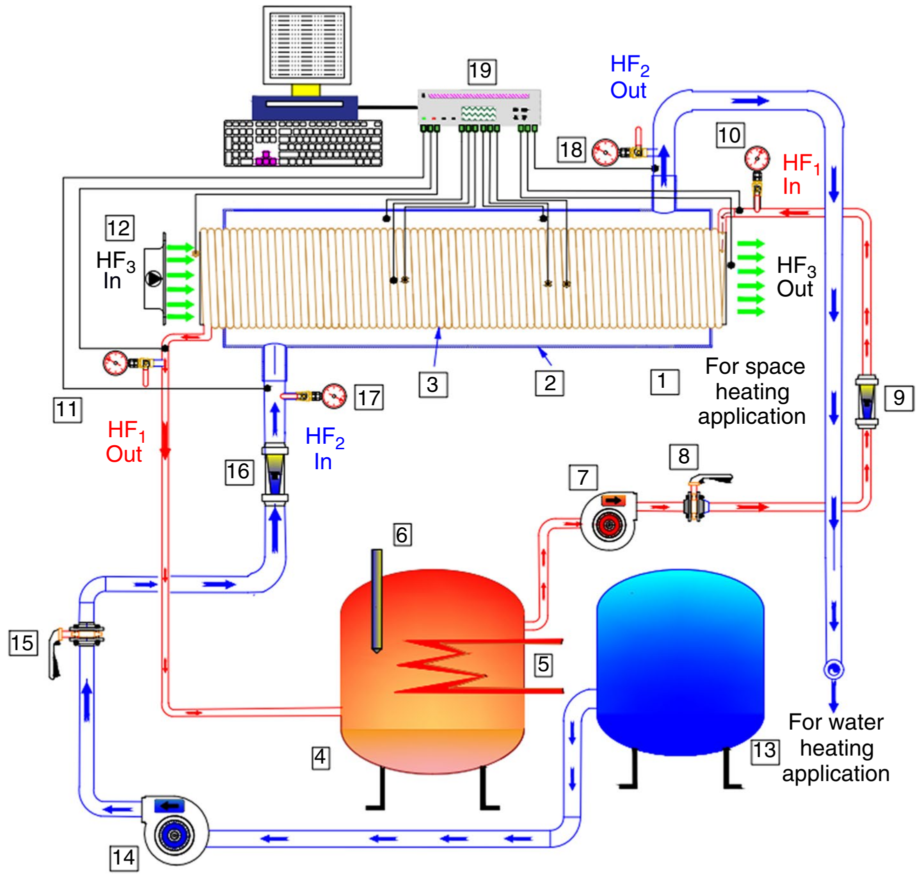

Fig. 1 Schematic layout of the NMFHE experimental setup. 1—Test section of NMFHE, 2—Shell, 3—Helical coil tube, 4—HF_1 tank, 5—Immersion heater (3 kW), 6—Thermostat, 7—Pump (HF_1), 8—Flow control valve (HF_1), 9—Rotameter (HF_1), 10—Inlet pressure gauge (HF_1), 11—Outlet pressure gauge (HF_1), 12—Fan, 13—HF_2 tank, 14—Pump (HF_2), 15—Flow control valve (HF_2), 16—Rotameter (HF_2), 17—Inlet pressure gauge (HF_2), 18—Outlet pressure gauge (HF_2), and 19—Data logger

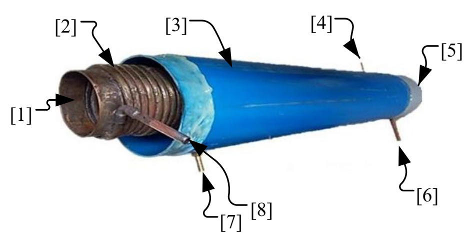

Fig. 2 NMFHE test section. 1—Hollow conduit of BHT, 2—Brazed helix tube (BHT), 3—Outer shell, 4—Shell outlet, 5—End cap, 6—Helical coil tube outlet, 7—Shell inlet, and 8—Helical coil tube inlet

and HF_2 (100 LPH, 150 LPH, and 200 LPH, respectively), three different flow velocities for HF_3 (1 m s^{-1}, 2 m s^{-1}, and 3 m s^{-1}), and three different inlet temperatures of HF_1 (333 K, 243 K, and 253 K). The inlet temperatures of HF_2 and HF_3 throughout the experimental procedure are kept constant. As shown in Fig. 3, the investigation makes use of all four flow configurations, including parallel flow (PF) and three different counter-flow configurations (CF1, CF2, and CF3). In the first flow configuration, all three fluids (HF_1, HF_2, and HF_3) flow in the same direction from right to left of the NMFHE test section. As shown in Fig. 3, the flow directions of the other two fluids are unaffected by the counter-flow configurations (CF1, CF2, and CF3); however, the flow directions of HF_1, HF_2, and HF_3 individually are reversed. HF_1, HF_2, and HF_3 are allowed to circulate for 25–30 min inside the NMFHE test section to maintain steady-state condition. Afterward, experimental readings are taken for further analysis, discussion, and optimization study.

Uncertainty analysis

Accurate measurements in scientific research are critical for reliable results. However, no instrument is perfect, so it is required to consider possible errors in the measuring instruments. In the context of the present study, three different instruments used for the measurement of temperatures, flow rates, and air velocity are added in Table 1 with their make and the least count.

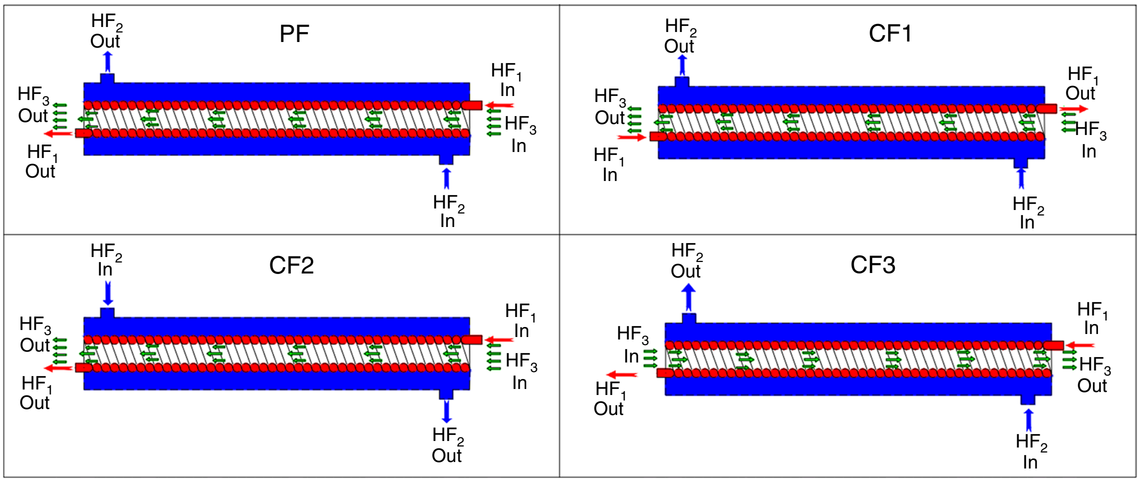

Fig. 3 Flow configuration diagram of the NMFHE

Table 1 Measuring instruments and least count

Instrument	Make	Least count
Thermocouples	Omega	±1.1C or 0.4%
Rotameter	Star flow technologies	±3% FSD
Anemometers	HTC anemometer	±5%rdg+0.5 dgts

Table 2 Uncertainty in output results

Output results	Uncertainty/%
JF factor (HF_1)	±0.0028
JF factor (HF_2)	±0.063
JF factor (HF_3)	±0.026
Entropy generation number of HF_1	±0.042
Entropy generation number of HF_2	±0.0002
Entropy generation number of HF_3	±0.0352

Ensuring the accuracy of the data gathered from the instruments equipped with NMFHE, it is necessary to calculate the uncertainty by using Eq. 1 [28]. The uncertainty values of output parameters are given in Table 2.

$$U_f = \sqrt{\left[\left(\frac{\partial f}{\partial x_1}\right).Ux_1\right]^2 + \left[\left(\frac{\partial f}{\partial x_2}\right).Ux_2\right]^2 + \left[\left(\frac{\partial f}{\partial x_3}\right).Ux_3\right]^2 + \ldots + \left[\left(\frac{\partial f}{\partial x_n}\right).Ux_n\right]^2} \quad (1)$$

Data reduction

The entropy generation and JF factor are calculated in the present study using the following formulas as mentioned in [29–31].

Entropy generation number

$$N_S = \frac{1}{\pi \cdot \mathrm{Nu}} + \frac{\pi^3 \cdot f \cdot \mathrm{Re}^5}{32 \cdot \left(\frac{(q')^2 \rho^2 \cdot \dot{m}^2}{K \cdot T \cdot \mu^5}\right)} \quad (2)$$

JF factor

$$\mathrm{JF} = \frac{j}{f^{1/3}} \quad (3)$$

Verification and validation of the present result

The findings of the present experimental work, i.e. Nusselt number for fluid flow inside the brazed helix tube (BHT), outer shell, and hollow conduit of NMFHE, are compared with Nusselt number correlations provided in the literature.

Figure 4a shows the verification of BHT side fluid (HF_1) Nusselt number with the Nusselt number correlations suggested by Rogers and Mayhew [32], i.e. is given in Eq. 4.

$$\mathrm{Nu}_{\mathrm{HF}_1} = 0.021\left(\mathrm{Re}_{\mathrm{HF}_1}\right)^{0.85}\left(\mathrm{Pr}_{\mathrm{HF}_1}\right)^{0.4}\left(\frac{d_{c,i}}{D_c}\right)^{0.1} \quad (4)$$

Figure 4b shows the verification of outer shell side fluid (HF_2) Nusselt number with the Nusselt number

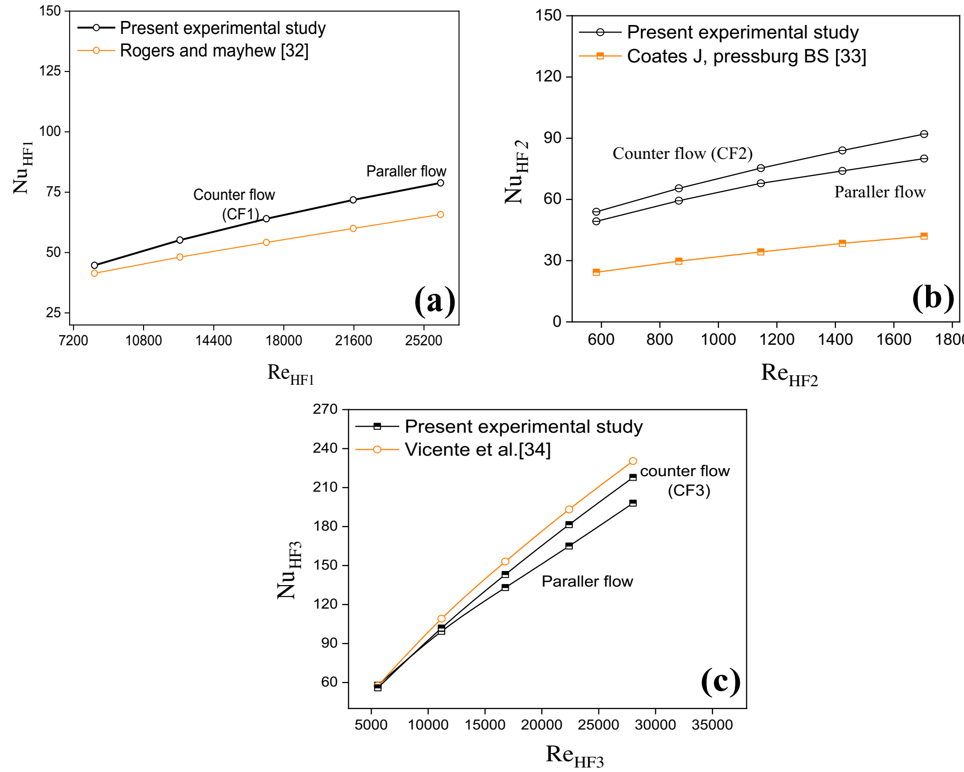

Fig. 4 The comparison of **a** helix tube, **b** outer shell side Nusselt number, and **c** hollow conduit side Nusselt number with the literature

correlations suggested by Coates and Pressburg [33], i.e. is given in Eq. 5.

$$Nu_{HF_2} = 0.6\, Re_{HF_2}^{0.5}\, Pr_{HF_2}^{0.31} \text{ for } 50 \le Re \le 10,000 \tag{5}$$

Figure 4c shows the verification of hollow conduit side fluid (HF_3) Nusselt number with the Nusselt number correlations suggested by Vicente et al. [34], i.e. is given in Eq. 6.

$$Nu = 0.374\left(\frac{h^2}{pd}\right)^{0.25}(Re - 1500)^{0.74}Pr^{0.44} \tag{6}$$

From Fig. 4a, b, and c, the results of the current experimental investigation appear to agreement reasonably well with those cited in the literature, this similarity helps confirm that our study is accurate. Differences in geometric configurations, thermal interactions, and the intrinsic surface corrugations present in both the shell side fluid (HF_2) and the fluid within the inner conduit (HF_3) may serve to clarify the minor divergences noted within the observed results.

Taguchi method

The Taguchi method forms the design of experiments technique that primarily tries to reduce the number of experimental repetitions while permitting the prediction of factor interactions, in order to determine particular optimized results. This technique constitutes an orthogonal array by reducing the number of experimental runs, thoroughly evaluating the influence of the investigated elements, providing signal-to-noise (S/N) analysis, and figuring out the best values for the variables under consideration. The performance optimization of heat exchangers can be accomplished successfully by combining the Taguchi method with Grey relational analysis. According to the literature, this collaborative strategy enables the systematic consideration of numerous input variables, producing economic efficiencies through the reduction of costs and experimental test runs [35–37].

The main steps of the Taguchi method are the selection of independent variables, level determination for each independent variable, selection of an orthogonal array that ensures a balanced comparison of levels, allocation of independent variables to individual columns, execution of the experiments, analytical interpretation of the data, and finally the formulation of conclusive insights. Notably, the minimum number of test runs necessary is derived from the total degrees of freedom (DF) [38] which is given in Eq. 7.

$$DF = Factors * (level - 1) \tag{7}$$

Calculated signal-to-noise (S/N) ratio serves as an indicator of the effectiveness of the experimental design by the Taguchi method. The resulting equations outline the formulas for several S/N ratio categories, including "larger-the-better" (LB), "smaller-the-better" (SB), and "nominal-the-better" (NB) conditions which are given in Eqs. 8, 9, and 10, respectively [39].

$$\mathrm{LB} = \frac{1}{n}\sum\left(\frac{1}{y_\mathrm{i}}\right)^2 \tag{8}$$

$$\mathrm{SB} = \frac{1}{n}\sum\left(y_\mathrm{i}\right)^2 \tag{9}$$

$$\mathrm{NB} = \frac{1}{n}\sum\left(y_\mathrm{i} - y_\mathrm{o}\right)^2 \tag{10}$$

Herein, "y" signifies the output variable, and "n" corresponds to the number of responses.

Equation 11 is used to calculate the value of the S/N ratio.

$$\mathrm{S/N\ ratio} = -10\log(L_\mathrm{i}) \tag{11}$$

where L_i is calculated from the formulas given in Eq. 12.

$$L_\mathrm{i}\begin{cases}\text{Larger is better} = \frac{1}{n}\sum_{i=1}^{n} 1/y_\mathrm{i}^2 \\ \text{Smaller is better} = \frac{1}{n}\sum_{i=1}^{n} y_\mathrm{i}^2\end{cases} \tag{12}$$

In the present study, the combined Taguchi method and Grey relational analysis are used to predict the optimal value of input parameters for the calculated optimized performance of the NMFHE. The control factors are mentioned in Table 3**.** These control factors include four principal operating flow parameters, specifically the HF_1 flow rate, the HF_2 flow rate, the HF_3 inlet temperature, and the flow configurations. The L18 orthogonal array for control factors, the experimental response, and the signal-to-noise ratio at different input parameters are shown in Table 4**.** Four control parameters: flow configuration, HF_1 flow rate, HF_2 flow rate, and HF_1 inlet temperature are the input variables that affect the performance of the heat exchanger in terms of entropy generation number (Ns) and JF factor for the optimization work by the Taguchi method. The Ns is analysed with "smaller is better". The JF factor is analysed with "larger is better".

Table 3 Control factors with their levels

Control factor	Level 1	Level 2	Level 3
Flow conf.	CF1	CF2	
HF_1 flow rate, LPH	100	150	200
HF_2 flow rate, LPH	100	150	200
HF_1 inlet temperature, K	333	343	353

Table 4 Taguchi response for JF factor and entropy generation number (Ns)

L18 orthogonal array					Experimental output responses					
Run	Flow conf. (A)	HF_1 flow rate (B)	HF_2 flow rate (C)	HF_1 inlet temp. (D)	JF factor (HF_1)	JF factor (HF2)	JF factor (HF3)	Ns (HF_1)	Ns (HF_2)	Ns (HF_3)
1	CF1	100	100	333	0.0076	0.0729	0.0260	0.0166	0.0077	0.0022
2	CF1	100	150	343	0.0085	0.0675	0.0405	0.0107	0.0064	0.0023
3	CF1	100	200	353	0.0089	0.0638	0.0398	0.0083	0.0056	0.0023
4	CF1	150	100	333	0.0052	0.0758	0.0266	0.0234	0.0075	0.0022
5	CF1	150	150	343	0.0059	0.0708	0.0417	0.0131	0.0062	0.0023
6	CF1	150	200	353	0.0061	0.0676	0.0413	0.0094	0.0054	0.0023
7	CF1	200	100	343	0.0031	0.0768	0.0340	0.0199	0.0073	0.0022
8	CF1	200	150	353	0.0035	0.0721	0.0424	0.0124	0.0060	0.0022
9	CF1	200	200	333	0.0048	0.0662	0.0291	0.0241	0.0053	0.0022
10	CF2	100	100	353	0.0067	0.0721	0.0446	0.0057	0.0009	0.0139
11	CF2	100	150	333	0.0097	0.0696	0.0443	0.0080	0.0008	0.0137
12	CF2	100	200	343	0.0105	0.0629	0.0954	0.0058	0.0007	0.0135
13	CF2	150	100	343	0.0048	0.0740	0.0444	0.0066	0.0009	0.0142
14	CF2	150	150	353	0.0055	0.0705	0.0959	0.0067	0.0008	0.0141
15	CF2	150	200	333	0.0076	0.0654	0.0443	0.0117	0.0007	0.0140
16	CF2	200	100	353	0.0028	0.0740	0.0444	0.0158	0.0009	0.0144
17	CF2	200	150	333	0.0043	0.0725	0.0443	0.0279	0.0008	0.0142
18	CF2	200	200	343	0.0046	0.0660	0.0485	0.0046	0.0007	0.0142

Table 5 Taguchi S/N ratio (dB) for JF factor and entropy generation number (Ns)

L18 orthogonal array					S/N ratio (dB)					
Run	Flow conf. (A)	HF_1 flow rate (B)	HF_2 flow rate (C)	HF_1 inlet temp. (D)	JF factor (HF_1)	JF factor (HF_2)	JF factor (HF_3)	Ns (HF_1)	Ns (HF_2)	Ns (HF_3)
1	CF1	100	100	333	0.008	0.073	0.026	0.017	0.008	0.002
2	CF1	100	150	343	0.008	0.067	0.041	0.011	0.006	0.002
3	CF1	100	200	353	0.009	0.064	0.040	0.008	0.006	0.002
4	CF1	150	100	333	0.005	0.076	0.027	0.023	0.007	0.002
5	CF1	150	150	343	0.006	0.071	0.042	0.013	0.006	0.002
6	CF1	150	200	353	0.006	0.068	0.041	0.009	0.005	0.002
7	CF1	200	100	343	0.003	0.077	0.034	0.020	0.007	0.002
8	CF1	200	150	353	0.003	0.072	0.042	0.012	0.006	0.002
9	CF1	200	200	333	0.005	0.066	0.029	0.024	0.005	0.002
10	CF2	100	100	353	0.007	0.072	0.045	0.006	0.001	0.014
11	CF2	100	150	333	0.010	0.070	0.044	0.008	0.001	0.014
12	CF2	100	200	343	0.011	0.063	0.095	0.006	0.001	0.013
13	CF2	150	100	343	0.005	0.074	0.044	0.007	0.001	0.014
14	CF2	150	150	353	0.005	0.071	0.096	0.007	0.001	0.014
15	CF2	150	200	333	0.008	0.065	0.044	0.012	0.001	0.014
16	CF2	200	100	353	0.003	0.074	0.044	0.016	0.001	0.014
17	CF2	200	150	333	0.004	0.073	0.044	0.028	0.001	0.014
18	CF2	200	200	343	0.005	0.066	0.048	0.005	0.001	0.014

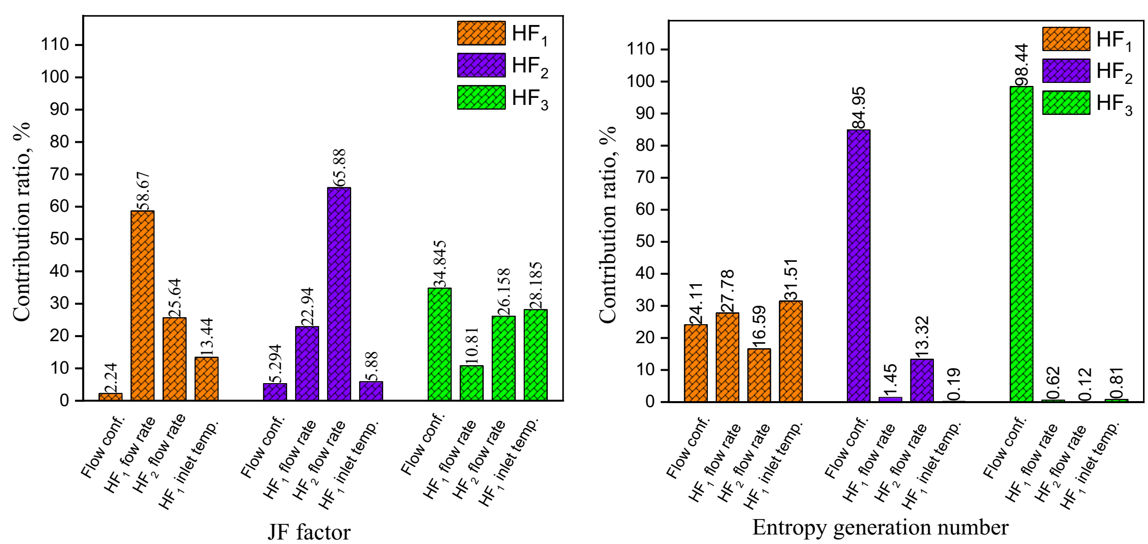

Fig. 5 Contribution ratio of each operating condition parameter to JF factor and entropy generation number (Ns)

The experimental response and S/N ratio for the JF factor and the entropy generation number, Ns are presented in Tables 4 and 5 in L18 orthogonal array.

The evaluation of the percentage contribution of each control parameter to the test performance is a crucial aspect of this study. This evaluation has been conducted using the signal-to-noise (S/N) ratio generated through the utilization of the Taguchi methodology. The resultant findings are graphically represented in Fig. 5**.** Within this analytical framework, the "delta" for each factor is defined and computed as the variance between the maximum and minimum S/N ratio values. Subsequently, the contribution rate is determined through a more intricate calculation. Specifically, the individual delta of each factor is subtracted from the collective sum of the deltas for all four factors.

From Taguchi analysis, the percentage contribution of each factor to the JF factor and Ns was determined for the NMFHE and is given in Fig. 5.

Grey relational analysis

GRA is generally useful for evaluating the relationship degree between sequences and Grey relational grade (GRG). GRA is commonly used to integrate all of the performance characteristics that are analysed into a single number, which is generally the solution to the optimization problem. There are two steps for solving GRA. In the first step, it is needed to convert the data into S/N ratio, and in the second step, the data are pre-processed by normalization of data in the range of zero and one. In the field of heat exchanger performance analysis, the application of GRA facilitates a thorough examination of the interplay between geometric and flow parameters. The Taguchi–Grey relational analysis (GRA) method is employed to investigate parameters such as the Reynolds number, pitch ratio, diameter ratio, etc. [40]. Within a concentric pipe heat exchanger system, corrugated tapes are utilized, and GRA aids in understanding the relationship between Nusselt number and friction factor. This enables the ordering of corrugated tapes based on their effect intensity concerning dimensions such as width, pitch, and thickness. Thickness emerges as the most critical component in terms of the friction factor [41]. They use Taguchi method to investigate various design parameters with a single-point response in order to improve the air-side performance of a wavy fin and tube heat exchanger. For consolidated optimization, which covers all targeted responses concurrently, the idea of Grey relational analysis, a subtle statistical method, is studied [42].

These normalized data are divided into two categories, one in which "larger is better" and in the other "smaller is better". If the output answer falls into the "bigger is better" group, it is stated using Eq. 13.

$$C_{\mathrm{i}}(e) = \frac{\left[x_{\mathrm{i}}(e)_{\max} - x_{\mathrm{i}}(e)\right]}{\left[x_{\mathrm{i}}(e) - x_{\mathrm{i}}(e)_{\min}\right]} \tag{13}$$

Herein, "$x_{\mathrm{i}}(e)$" represents the original sequence, whereas "$C_{\mathrm{i}}(e)$" sequence for comparing, with "i" ranging from 1 to n and "e" ranging from 1 to m. If the result falls in "smaller is better" category, then Eq. 14 may be considered

$$C_{\mathrm{i}}(e) = \frac{\left[x_{\mathrm{i}}(e) - x_{\mathrm{i}}(e)_{\max}\right]}{\left[x_{\mathrm{i}}(e)_{\max} - x_{\mathrm{i}}(e)_{\min}\right]} \tag{14}$$

Following the normalization of the sequence, the deviation of the sequence for all outputs is determined, and the Grey relational coefficient (GRC) was calculated by using the relationship provided in Eq. 15.

$$\mathrm{GRG} = \frac{d_{\min} + \psi d_{\max}}{d_{\mathrm{oi}} + \psi d_{\max}} \tag{15}$$

In this context, "d_{oi}" represents deviation of sequences across all responses. The highest and lowest deviation among all the compared sequences are designated as "$d_{\max}$" and "$d_{\min}$", respectively. The identification coefficient (Ψ) values between 0 and 1 assume a value of 0.5 in the current study. The Grey relational grade (GRG) is calculated by Eq. 16.

$$\mathrm{GRG} = \frac{\sum_{e=1}^{e=m} \mathrm{GRC}}{m} \tag{16}$$

Results and discussion

Model prediction and analysis of variance

The optimization software uses linear regression analysis as a function of input parameters to create a linear mathematical model for various output responses. The resultant mathematical equations for each respective response are presented, from Eq. 17 to Eq. 22. These predictive equations were formulated specifically for the JF factor ($\mathrm{HF_1}$), JF factor (HF2), JF factor (HF3), Ns (HF1), Ns (HF2), and Ns (HF3).

$$\begin{cases} \text{CF1, JF factor }(\mathrm{HF_1}) = 0.01339 - 0.000048\ \mathrm{HF_1}\text{ flow rate} + 0.00002\ \mathrm{HF_2}\text{ flow rate} - 0.000048\ \mathrm{HF_1}\text{ Inlet temp.} \\ \text{CF2, JF factor }(\mathrm{HF_1}) = 0.0137 - 0.000048\ \mathrm{HF_1}\text{ flow rate} + 0.00002\ \mathrm{HF_2}\text{ flow rate} - 0.000048\ \mathrm{HF_1}\text{ Inlet temp.} \end{cases} \tag{17}$$

$$\begin{cases} \text{CF1, JF factor }(\mathrm{HF_2}) = 0.08047 + 0.000031\ \mathrm{HF_1}\text{ flow rate} - 0.00009\ \mathrm{HF_2}\text{ flow rate} - 0.000019\ \mathrm{HF_1}\text{ Inlet temp.} \\ \text{CF2, JF factor }(\mathrm{HF_2}) = 0.07977 + 0.000031\ \mathrm{HF_1}\text{ flow rate} - 0.00009\ \mathrm{HF_2}\text{ flow rate} - 0.000019\ \mathrm{HF_1}\text{ Inlet temp.} \end{cases} \tag{18}$$

$$\begin{cases} \text{CF1, JF factor }(\mathrm{HF_3}) = -0.0266 - 0.00008\ \mathrm{HF_1}\text{ flow rate} + 0.000131\ \mathrm{HF_2}\text{ flow rate} + 0.000781\ \mathrm{HF_1}\text{ Inlet temp.} \\ \text{CF2, JF factor }(\mathrm{HF_3}) = -0.006 - 0.00008\ \mathrm{HF_1}\text{ flow rate} + 0.000131\ \mathrm{HF_2}\text{ flow rate} + 0.000781\ \mathrm{HF_1}\text{ Inlet temp.} \end{cases} \tag{19}$$

Table 6 ANOVA analysis and model prediction

Source	DF	JF factor (HF_1)		JF factor (HF_2)		JF factor (HF_3)		Ns (HF_1)		Ns (HF_2)		Ns (HF_3)	
		F-value	P-value	*F*-value	P-value	*F*-value	P-value	*F*-value	P-value	*F*-value	P-value	*F*-value	P-value
ANOVA analysis													
Flow conf.	1	2.4	0.152	2.39	0.153	7.96	0.02	6.81	0.026	851.6	0	18,091	0
HF_1 flow rate	2	192.2	0	17.67	0.001	0.58	0.58	6.52	0.015	0.32	0.734	3.14	0.09
HF_2 flow rate	2	34.79	0	129.5	0	1.65	0.24	1.5	0.27	12.45	0.002	0.73	0.51
HF_1 inlet temp.	2	7.94	0.009	0.88	0.443	1.96	0.19	9.22	0.005	2.67	0.118	0.56	0.59

	JF factor (HF_1), %	JF factor (HF_2), %	JF factor (HF_3), %	Ns (HF_1), %	Ns (HF_2), %	Ns (HF_3), %
Model prediction						
R-sq	97.93	96.76	94.05	89.51	98.88	99.94
R-sq(adj)	96.47	94.49	92.49	86.86	98.10	99.91
R-sq(pred)	93.28	89.49	90.01	86.84	96.37	99.82

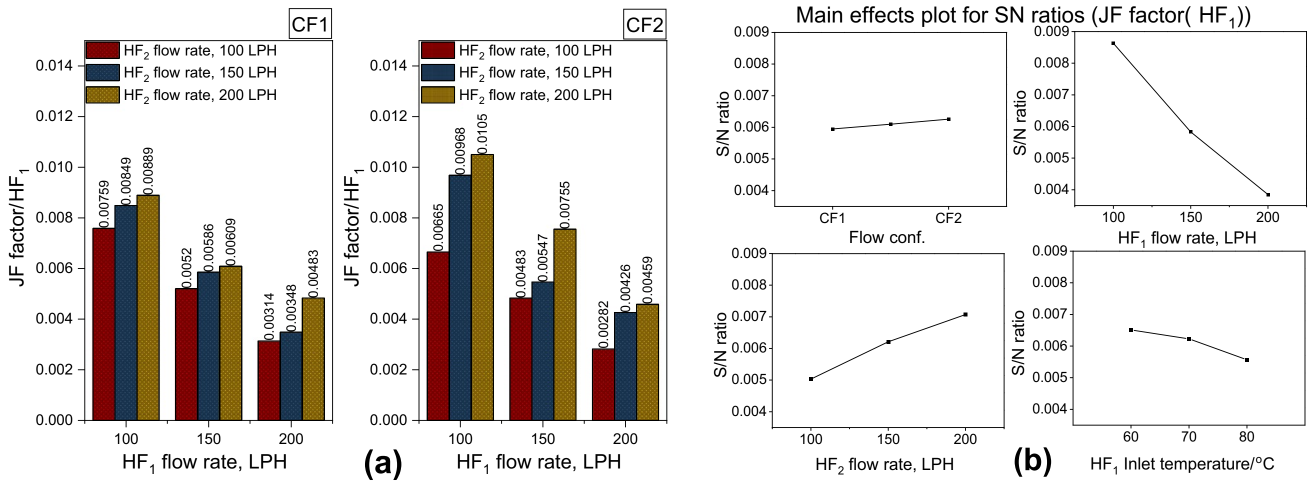

Fig. 6 Effect of each input parameter on the JF factor (HF_1)

$$\begin{cases} \text{CF1, Ns } (HF_1)=0.0401+0.000083\ HF_1 \text{ flow rate}-0.00004\ HF_2 \text{ flow rate}-0.000445\ HF_1 \text{ Inlet temp.} \\ \text{CF2, Ns } (HF_1)=0.0351+0.000083\ HF_1 \text{ flow rate}-0.00004\ HF_2 \text{ flow rate}-0.000445\ HF_1 \text{ Inlet temp.} \end{cases} \quad (20)$$

$$\begin{cases} \text{CF1, Ns } (HF_2)=0.0102-0.000002\ HF_1 \text{ flow rate}-0.000012\ HF_2 \text{ flow rate}-0.000025\ HF_1 \text{ Inlet temp.} \\ \text{CF2, Ns } (HF_2)=0.0046-0.000002\ HF_1 \text{ flow rate}-0.000012\ HF_2 \text{ flow rate}-0.000025\ HF_1 \text{ Inlet temp.} \end{cases} \quad (21)$$

$$\begin{cases} \text{CF1, Ns } (HF_3)=0.0017+0.000003\ HF_1 \text{ flow rate}-0.000001\ HF_2 \text{ flow rate}-0.000005\ HF_1 \text{ Inlet temp.} \\ \text{CF2, Ns } (HF_3)=0.0135+0.000003\ HF_1 \text{ flow rate}-0.000001\ HF_2 \text{ flow rate}-0.000005\ HF_1 \text{ Inlet temp.} \end{cases} \quad (22)$$

The R^2-value shows the capability of the model to predict output responses, which vary from 0 to 1. The R^2-value close to 1 or more than 90% shows a good model fit to relate the independent and dependent variables effectively. The models formulated for the JF factor (HF_1, HF_2, and HF_3), as well as the entropy generation number for HF_1, HF_2, and HF_3, are detailed in the analysis of variance (ANOVA) presented in Table 6. The respective R^2-values for these models are 97.93%, 96.76%, 94.05%, 89.51%, 98.88%, and 99.94%. Such results underscore the models' high precision and dependability in forecasting the output responses.

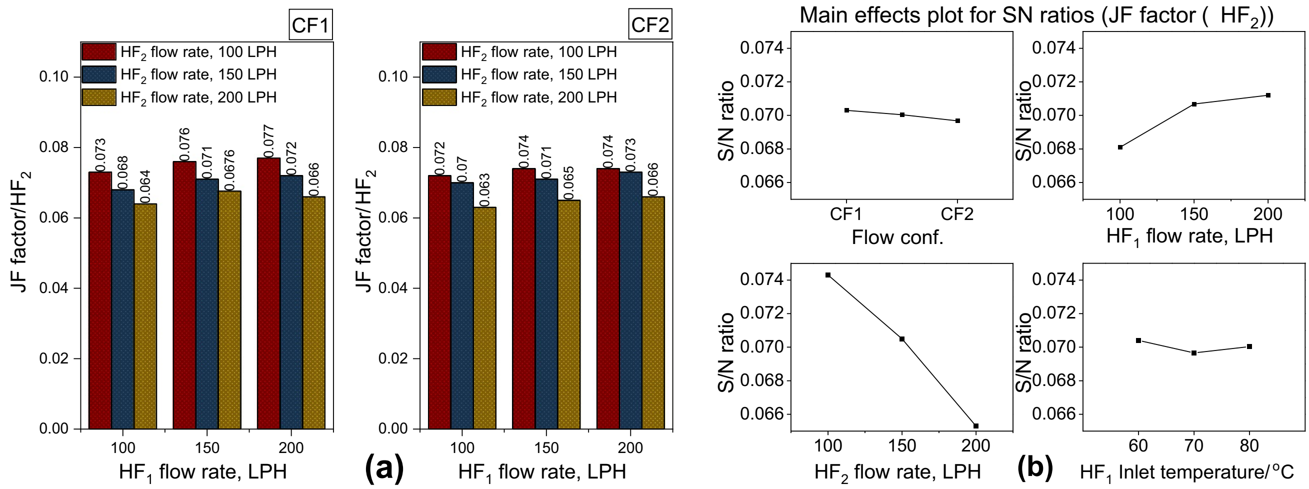

Fig. 7 Effect of each input parameter on JF factor (HF_2)

Effect of control factors on output responses

JF factor (HF_1)

Figure 6 shows the effect of flow configuration, HF_1 inlet temperature, HF_1 flow rate, and HF_2 flow rate on JF factor (HF_1). It is observed in Fig. 6a that the maximum JF factor (HF_1) is achieved at CF2 flow configuration, 100 LPH flow rate of HF_1, 200 LPH flow rate of HF_2, and 333 K inlet temperature of HF_1. This finding is consistent with the results presented in Fig. 6b. Notably, the HF_1 flow rate has a substantial impact on JF factor (HF_1) which is confirmed in Figs. 5 and 6b with a contribution of 58.67%, followed by the HF_2 flow rate, HF_1 inlet temperature, and flow configuration with contribution of 25.64%, 13.44%, and 2.24%, respectively. The NMFHE performs better in CF2 flow configuration, as the bulk mean temperature of HF_1 is higher compared to HF_2 and HF_3. It is noticed that increment in volumetric flow rate of HF_1 and HF_2 decreases JF factor (HF_1), as increased flow rate leads to more turbulence and more heat transfer. However, the influence of HF_1 inlet temperature on JF factor (HF_1) is minimal as the variation of temperature is limited to 283 K, which increases the thermo-physical properties of the HF_1 slightly. Insignificant changes in thermo-physical properties may be a cause of this result.

JF factor (HF_2)

Figure 7 shows the effect of flow configuration, HF_1 inlet temperature, HF_1 flow rate, and HF_2 flow rate on JF factor

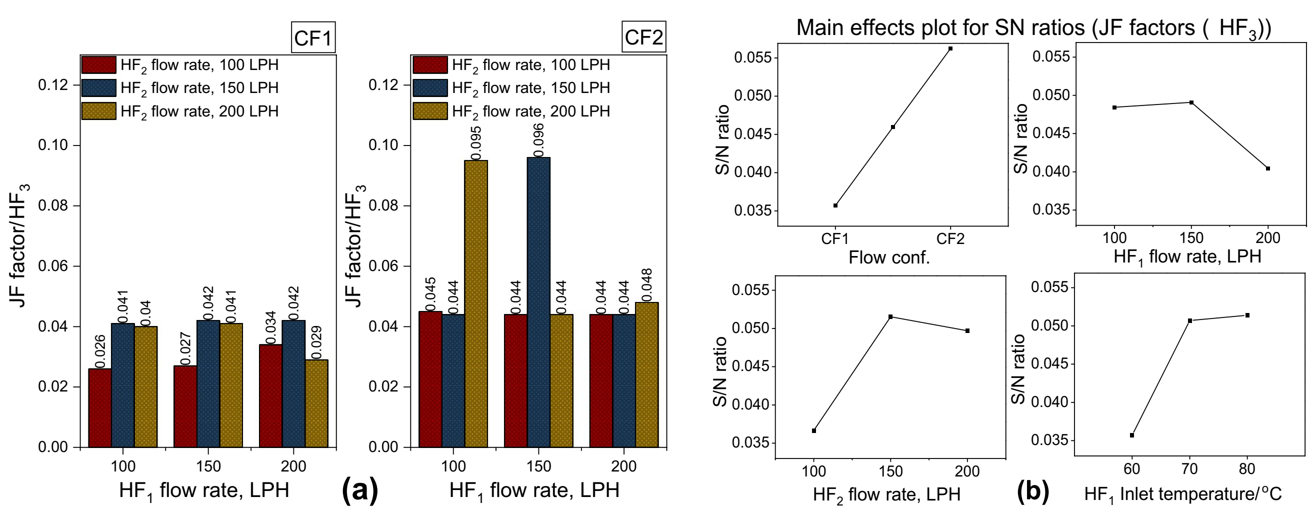

Fig. 8 Effect of each input parameter on JF factor (HF_3)

(HF_2). Figure 7b shows the S/N ratio plot which indicates higher heat transfer performance of the present NMFHE at higher value of S/N ratio. It is observed in Fig. 7b that the maximum JF factor (HF_2) is achieved at CF1 flow configuration, 200 LPH flow rate of HF_1, 100 LPH flow rate of HF_2, and 333 K inlet temperature of HF_1. This finding is consistent with the results presented in Fig. 7a. Notably, the HF_2 flow rate has a substantial impact on JF factor (HF_2) which is confirmed in Figs. 5 and 7b with a contribution of 65.88%, followed by the HF_1 flow rate, HF_1 inlet temperature, and flow configuration with contribution of 22.94%, 5.88%, and 5.294%, respectively. The NMFHE performs better in CF1 flow configuration, as the bulk quantity of HF_2 is higher compared to HF_1 and HF_3. So, its reversal also affects that the most is stated above. It is noticed that increment in volumetric flow rate of HF_1 and HF_2 increases JF factor (HF_2), as increased flow rate leads to more turbulence and more heat transfer. However, the influence of HF_1 inlet temperature on JF factor (HF_2) is minimal as the variation of temperature is limited to 283 K, which slightly increases the thermo-physical properties of the HF_1. Insignificant changes in thermo-physical properties could be a cause of this result.

JF factor (HF_3)

Figure 8 shows the effect of flow configuration, HF_1 inlet temperature, HF_1 flow rate, and HF_2 flow rate on JF factor (HF_3). Specifically, Fig. 8b shows the S/N ratio plot which indicates higher heat transfer performance of the present NMFHE at higher value of S/N ratio. It is observed in Fig. 8b that the maximum JF factor (HF_3) is achieved at CF2 flow configuration, 150 LPH flow rate of HF_1, 150 LPH flow rate of HF_2, and 353 K inlet temperature of HF_1. This finding is consistent with the results presented in Fig. 8a. Notably, the flow configuration has a substantial impact on JF factor (HF_3) which is confirmed in Figs. 5 and 8b with a contribution of 34.85%, followed by the HF_1 inlet temperature, HF_2 flow rate, and HF_1 flow rate with contribution of 28.19%, 26.16%, and 10.81%, respectively. The NMFHE performs better in CF2 flow configuration, as the bulk quantity of HF_2 is higher compared to HF_1 and HF_3. So, its reversal also affects that the most is stated above. It is noticed that increment in volumetric flow rate of HF_1 increases JF factor (HF_3), as increased flow rate leads to more turbulence and more heat transfer. However, the influence of HF_1 inlet temperature on JF factor (HF_3) is minimal as the variation of temperature is limited to 283 K, which slightly increases the thermo-physical properties of the HF_1. Insignificant changes in thermo-physical properties may be a cause of this result.

Entropy generation number of HF_1

In Fig. 9, the effect of flow configuration, flow rate of HF_1, flow rate of HF_2, and inlet temperature of HF_1 on entropy generation number of HF_1, Ns (HF_1) is presented. The result indicates that for the "smaller is better" statement, the minimum value of Ns (HF_1) is obtained at the HF_1 flow rate of 100 LPH, HF_2 flow rate of 200 LPH, HF_1 inlet temperature of 343 K, and flow configuration of CF2. This finding is consistent with the results presented in Fig. 9b. Notably, the HF_1 inlet temperature is found out as the most contributing factor as shown in Figs. 5 and 9b with a contribution of 31.51% followed by the HF_1 flow rate, flow configuration, and HF_2 flow rate contribute 27.78%, 24.11%, and 16.59%, respectively. The HF_1 flow rate has a significant impact on Ns (HF_1) as illustrated in Fig. 9. This is because at higher

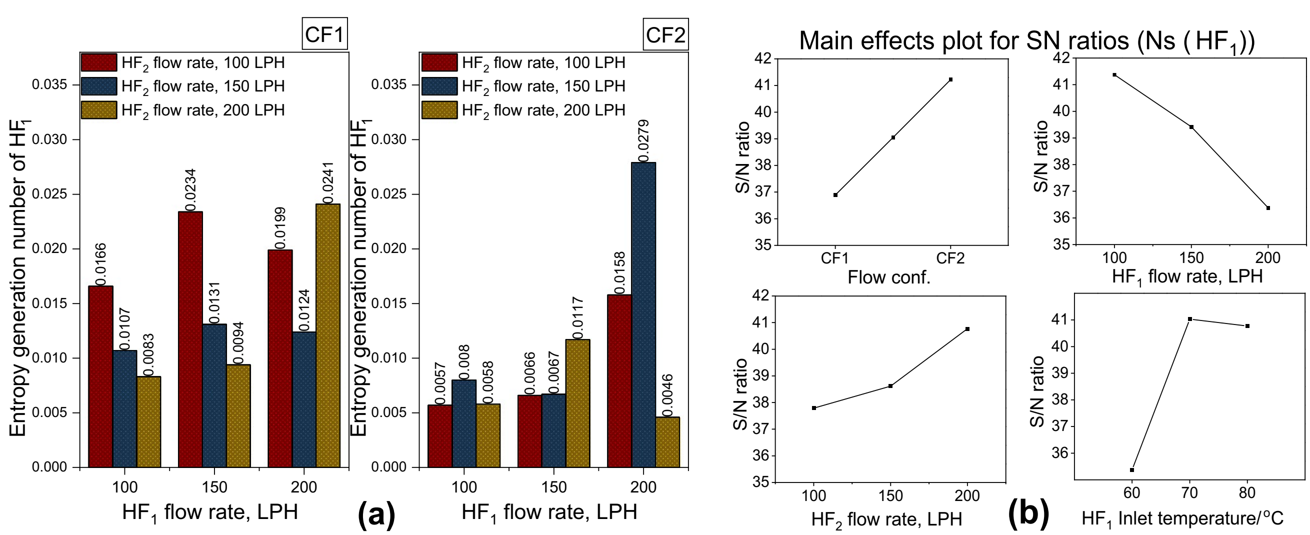

Fig. 9 Effect of each input parameter on entropy generation number of HF_1

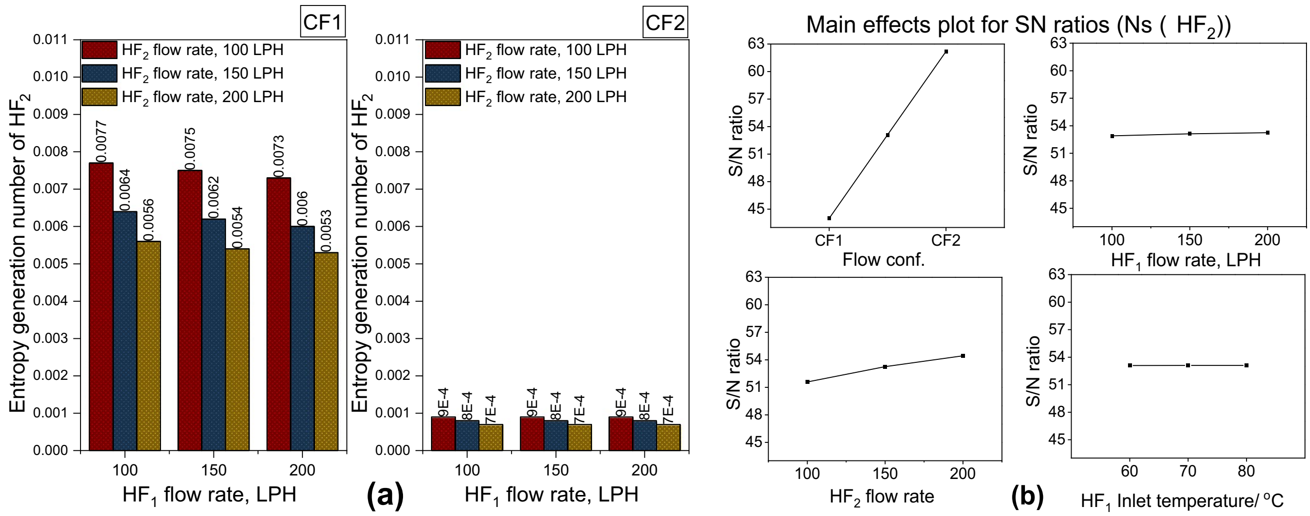

Fig. 10 Effect of each input parameter on *e*ntropy generation number of HF_2

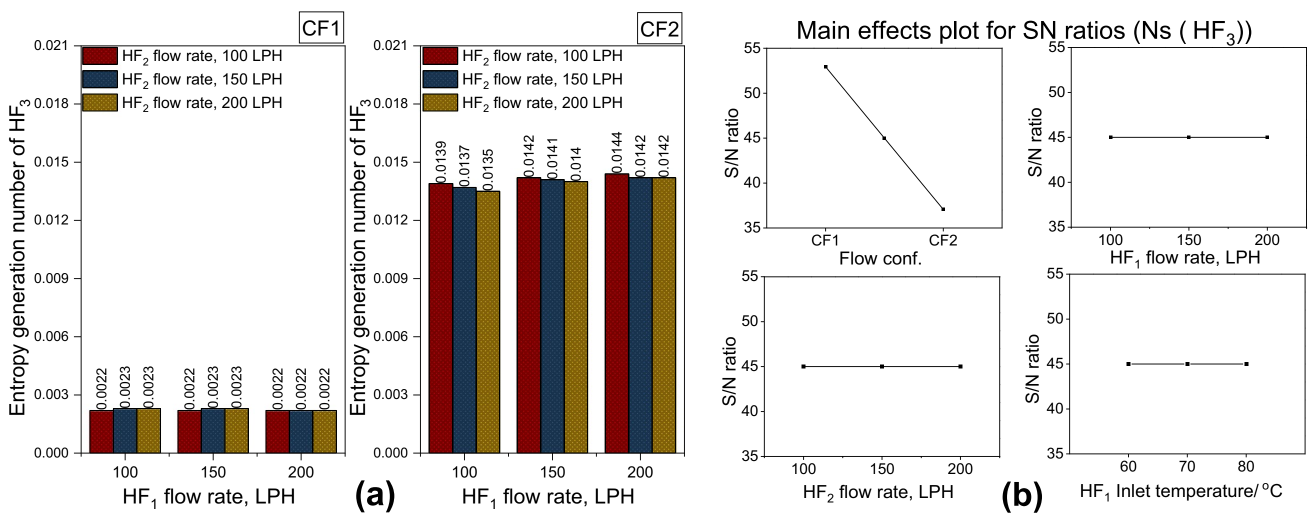

Fig. 11 Effect of each input parameter on entropy generation number of HF_3

flow rates, the resultant turbulence is more which causes more pressure drop.

Entropy generation number of HF_2

In Fig. 10, the effect of flow configuration, flow rate of HF_1, flow rate of HF_2, and inlet temperature of HF_1 on entropy generation number of HF_2, Ns (HF_2) is presented. The result indicates that for the "smaller is better" statement, the minimum value of Ns (HF_2) is obtained at the HF_1 flow rate of 200 LPH, HF_2 flow rate of 200 LPH, HF_1 inlet temperature of 353 K, and flow conf. of CF2. There is little effect of flow configuration on Ns (HF_2). A slight change in value of Ns (HF_2) due to a change in the HF_1 inlet temperature and HF_1 flow rate. This finding is consistent with the results presented in Fig. 10**.** Notably, the flow conf. is found out as the most contributing factor as shown in Figs. 5 and 10b with a contribution of 84.95% followed by the flow rate of $HF_{2,}$ flow rate of HF_1, and inlet temperature of HF_1 configuration contribute 13.32%, 1.54%, and 0.19%, respectively. The HF_2 flow rate has a significant impact on Ns (HF_2) as illustrated in Fig. 10. This is because at higher flow rates, the chaotic motion of HF_2 during flow over the corrugated surface of BHT causes more pressure drop.

Entropy generation number of HF_3

In Fig. 11, the effect of flow configuration, flow rate of HF_1, flow rate of HF_2, and inlet temperature of HF_1 on entropy generation number of HF_3, Ns (HF_3) is presented. The result

Table 7 Normalized and deviation sequences

Sl. No.	Normalized value						Deviation sequences					
	JF factor (HF_1)	JF factor (HF_2)	JF factor (HF_3)	Ns (HF_1)	Ns (HF_2)	Ns (HF_3)	JF factor (HF_1)	JF factor (HF_2)	JF factor (HF_3)	Ns (HF_1)	Ns (HF_2)	Ns (HF_3)
1	0.738	0.328	0.207	0.741	0.18	1	0.38	0.282	1	0.51	1	0.001
2	0.79	0.061	0.196	0.844	0.29	0.99	0.262	0.672	0.793	0.26	0.82	0.004
3	0.31	0.928	0.008	0.193	0.03	1	0.21	0.939	0.804	0.16	0.71	0.007
4	0.395	0.565	0.224	0.635	0.22	1	0.69	0.072	0.992	0.81	0.97	0
5	0.425	0.338	0.218	0.798	0.33	1	0.605	0.435	0.776	0.37	0.78	0.002
6	0.041	1	0.113	0.346	0.05	1	0.575	0.662	0.782	0.2	0.67	0.004
7	0.086	0.662	0.234	0.667	0.24	1	0.959	0	0.887	0.65	0.95	0
8	0.262	0.238	0.044	0.162	0.34	1	0.914	0.338	0.766	0.33	0.76	0.002
9	0.499	0.664	0.265	0.954	0.96	0.04	0.738	0.762	0.956	0.84	0.66	0
10	0.893	0.484	0.261	0.856	0.98	0.06	0.501	0.336	0.735	0.05	0.04	0.959
11	1	0	0.992	0.951	1	0.07	0.107	0.516	0.739	0.14	0.02	0.944
12	0.262	0.8	0.263	0.917	0.96	0.02	0	1	0.008	0.05	0	0.926
13	0.345	0.547	1	0.91	0.99	0.03	0.738	0.2	0.737	0.08	0.04	0.985
14	0.616	0.175	0.262	0.696	1	0.04	0.655	0.453	0	0.09	0.01	0.974
15	0	0.8	0.263	0.519	0.96	0	0.384	0.825	0.738	0.3	0	0.964
16	0.187	0.69	0.262	0	0.99	0.01	1	0.2	0.737	0.48	0.04	1
17	0.229	0.22	0.321	1	1	0.02	0.813	0.31	0.738	1	0.02	0.988
18	0.229	0.22	0.321	1	1	0.02	0.771	0.78	0.679	0	0	0.981

Table 8 Grey relation coefficient and grade

Run	Grey relation coefficient						Grey relation grade	S/N ratio	Rank
	JF factor (HF_1)	JF factor (HF_2)	JF factor (HF_3)	Ns (HF_1)	Ns (HF_2)	Ns (HF_3)			
1	0.568	0.639	0.333	0.493	0.333	0.997	0.561	−0.00017	11
2	0.656	0.427	0.387	0.659	0.380	0.992	0.583	0.022335	8
3	0.704	0.348	0.384	0.762	0.414	0.986	0.600	0.038711	6
4	0.420	0.875	0.335	0.383	0.340	1.000	0.559	−0.00225	12
5	0.452	0.534	0.392	0.578	0.389	0.996	0.557	−0.00393	13
6	0.465	0.430	0.390	0.712	0.426	0.992	0.569	0.008286	10
7	0.343	1.000	0.361	0.433	0.345	0.999	0.580	0.019185	9
8	0.354	0.596	0.395	0.600	0.396	0.996	0.556	−0.00478	14
9	0.404	0.396	0.343	0.374	0.430	0.999	0.491	−0.06993	18
10	0.499	0.598	0.405	0.915	0.926	0.343	0.614	0.053369	4
11	0.824	0.492	0.404	0.777	0.965	0.346	0.635	0.073683	3
12	1.000	0.333	0.985	0.912	0.996	0.351	0.763	0.201682	1
13	0.404	0.714	0.404	0.858	0.926	0.337	0.607	0.046239	5
14	0.433	0.524	1.000	0.848	0.972	0.339	0.686	0.125162	2
15	0.565	0.377	0.404	0.622	0.997	0.342	0.551	−0.00975	15
16	0.333	0.714	0.404	0.510	0.930	0.333	0.537	−0.02355	16
17	0.381	0.617	0.404	0.333	0.970	0.336	0.507	−0.05403	17
18	0.394	0.391	0.424	1.000	1.000	0.338	0.591	0.029963	7

Table 9 Response table of GRGs and its peak values

Factors	Level 1	Level 2	Level 3	Delta	Rank
Flow conf.	0.5618	**0.6102**		0.0484	3
HF_1 flow rate	**0.6259**	0.5883	0.5438	0.0821	1
HF_2 flow rate	0.5765	0.5874	**0.5942**	0.0177	4
HF_1 inlet temp.	0.5506	**0.6136**	0.5939	0.063	2

Mean of GRG = 0.586

indicates that for the "smaller is better" statement, the minimum value of Ns (HF_3) is obtained at the HF_1 flow rate of 200 LPH, flow configuration of CF1, HF_2 flow rate of 100 LPH, and HF_1 inlet temperature of 353 K. This finding is consistent with the results presented in Fig. 11. Notably, the flow conf. is found out as the most contributing factor as shown in Figs. 5 and 11b with a contribution of 98.44% followed by the inlet temperature of HF_1, HF_1 flow rate, and flow rate of HF_2 contribute 0.81%, 0.62%, and 0.12%, respectively.

Taguchi–Grey technique for multiple performance optimizations

In the present research, a methodological application of Taguchi–Grey analysis has been employed to perform multiple response optimizations for a NMFHE. The primary objectives encompass maximizing the heat transfer performance, characterized by the JF factor, and minimizing the hydraulic performance, denoted by Ns. A thorough examination of signal-to-noise (S/N) ratios is conducted, and the results are tabulated in Table 5. Subsequent preprocessing and normalization of the data are performed using

Table 10 Analysis of variance

Source	DF	Adj SS	Adj MS	*F*-value	P-value	% contribution
Flow conf.	1	0.010528	0.010528	4.56	0.059	1.56
HF1 flow rate	2	0.023281	0.01014	4.39	0.043	34.58
HF2 flow rate	2	0.000956	0.000478	0.21	0.816	0.142
HF1 inlet temp.	2	0.012565	0.006229	2.7	0.116	18.66
Error	10	0.02	0.002311			
Total	17	0.06733				
S	*R*-sq	*R*-sq(adj)	*R*-sq(pred)			
0.04807	92.46%	91.68%	90.77%			

Table 11 Result of the confirmation test

Initial design parameters		Optimal design parameters	
		Prediction	Experiment
Setting level	CF1, HF_1 flow rate 1, HF_2 flow rate 2, HF_1 inlet temp. 2	CF2, HF_1 flow rate 2, HF_2 flow rate 2, HF_1 inlet temp. 3	CF2, HF_1 flow rate 2, HF_2 flow rate 2, HF_1 inlet temp. 3
Grey relation grade	0.586	0.686	0.635
Improvement in GRG		17.17%	**8.36%**

Eqs. 14 and 15, and the corresponding normalized values and deviation sequences are cataloged in Table 7. Following this preprocessing stage, the deviation sequence Grey relational coefficient (GRC) is systematically calculated for each response using Eq. 15. Additionally, the Grey relational grade (GRG) is determined via Eq. 16, with these computations presented in Table 8. Within this framework, the highest S/N ratio serves as an indicator of the top-ranked factor, specifically correlated to the 12th experimental run.

After assigning these rankings, a response table for Grey relational grade (GRG) is formulated, facilitating a thorough examination of GRG across the factors. This involves calculating the mean GRG for each factor by averaging the individual GRG values at their specified levels. As depicted in Table 8, there exists an identifiable correlation between the reference sequence and the GRG compatibility sequence. Higher mean GRG values are indicative of higher correlations, thereby providing significant insights into the interactions of the variables within the NMFHE system. The peak GRG value is recorded at level 3 for the HF_2 flow rate, level 2 for the flow configuration, level 1 for the HF_1 flow rate, and level 2 for the HF_1 inlet temperature, as delineated in Table 9. Consequently, the optimal performance of the NMFHE is achieved with the CF2 flow configuration, an HF_2 flow rate of 200 LPH, an HF_1 flow rate of 100 LPH, and an HF_1 inlet temperature of 343 K.

Analysis of variance for GRG

To evaluate the influence of the parameters on the response outcomes, an analysis of variance (ANOVA) was executed for the GRG at a significance level of 5%. Subsequently, the proportional contribution of each parameter was ascertained and is tabulated in Table 10**.** The findings underscore that the HF_1 flow rate exerts the most pronounced effect with a contribution of 34.58%. This is followed by the HF_1 inlet temperature, flow configuration, and HF_2 flow rate, with contributions of 18.66%, 1.56%, and 0.142%, respectively. Additionally, the R^2-value surpassed 92.46%, suggesting a robust correlation between the GRG model and the observed data.

Confirmation test and improvement in GRG

The next phase involves anticipating and verifying the quality attributes using Eq. 23 after determining the ideal conditions using Grey analysis:

$$\text{GRG}_{\text{predicted}} = \text{GRG}_{\text{mean}} + \sum_{i=1}^{q} \left(\text{GRG}_{\text{oi}} - \text{GRG}_{\text{mean}}\right) \quad (23)$$

Herein, q signifies the number of components, GRG_{oi} is indicative of the highest value of the mean GRG, and GRG $_{\text{mean}}$ represents the median GRG value.

The GRG prediction is effectuated through Eq. 23, followed by the execution of a validation test to affirm the outcomes. The preliminary condition parameters are discerned by referencing the average value from the GRG dataset, subsequently opting for the GRG value in Table 9 that most closely approximates this mean value.

Table 11 represents that the expected values and the results of the confirmation test are close to each other. This shows that the optimization process is reliable. The Grey relational grade (GRG) is improved by 8.36% which has been confirmed, which indicates that the combine Taguchi technique and Grey relational analysis efficiently improve the performance of the NMFHE.

Conclusions

A detailed study of the thermo-hydraulic and exergetic performance of the NMFHE is carried out presently by varying different input parameters such as flow configuration, flow rate, and inlet temperature. Currently, the JF factor and entropy generation number, Ns, are determined as the output responses. With the Taguchi method, an L18 orthogonal array is used for conducting experimental runs, and the overall performance of the NMFHE is optimized, i.e. maximum JF factor and minimum Ns determined in regard to the optimal value of input parameters using the Grey relational grade technique in %. Based on the results, the following conclusions have been drawn.

i. Variation in flow configuration from CF1 to CF2 resulted higher JF factor*s* for HF_1 and HF_3, as well as higher Ns for HF_1 and HF_2. Conversely, the JF factor (HF_2) and the Ns value for HF_3 decrease with variation in flow configuration from CF1 to CF2. The CF2 flow configuration is identified as the most significant factor to the JF factor (HF_3) and the Ns value of HF_3 with a contribution of 34.86% and 98.44% of the total variation, respectively.
ii. Increasing the flow rate of HF_1 resulted in an increased JF factor (HF_2) but decreased JF factor (HF_1) and Ns (HF_1). The JF factor (HF_3) showed an initial rise followed by a decline. Minimal changes were seen for Ns (HF_2) and (HF_3). Notably, the *JF factor* (HF_1) and the Ns value of HF_1 were significantly impacted, accounting for 58.67% and 27.78% of the total variation, respectively.
iii. With an increase in the flow rate of HF_2, the JF factor (HF_1), Ns (HF_1), and Ns (HF_2) increase significantly, while the JF factor (HF_2) decreases significantly, with negligible changes observed for Ns (HF_3). The JF factor (HF_3) increases initially and decreases later. The HF_2 flow rate is identified as the most significant factor to JF factor (HF_2) and Ns (HF_1) with a contribution of 65.88% and 16.59% of the total variation, respectively.
iv. With an increase in the HF_1 inlet temperature, the JF factor (HF_3) increases and the JF factor (HF_1) decreases significantly, whereas negligible changes are observed for the Ns (HF_2) and Ns (HF_3). HF_1 inlet temperature is identified as the most significant factor for the JF factor (HF_3) and Ns (HF_1) with a contribution of 28.18% and 31.51% of the total variation, respectively.
v. A confirmation test was performed to validate the results of the optimization analysis. An improvement of 8.36% in performance was observed with the considered GRG model.
vi. Performance optimization of the NMFHE was conducted using the Taguchi—GRA method. The CF2 flow configuration, 150 LPH of HF_1 flow rate, 150 LPH of HF_2 flow rate, and 80 °C of HF1 inlet temperature were found as the optimum input parameters for this study
vii. The performance of the NMFHE can be tested with nanofluids for improved heat transfer performance. The numerical analysis could be performed by varying geometrical parameters at different fluid flow conditions. These are the possible future scopes of this study.

Acknowledgements This study has not been supported or funded by any organization or institution.

Author contributions BA experimented on the test setup, collected and analysed the data, and wrote the initial draft of the manuscript. TM contributed to the design and fabrication of the test setup and conducted overall performance optimization analysis. SSM provided expertise in critical revisions to the manuscript and assisted with data interpretation. All authors reviewed and approved the final version of the manuscript. This statement shows the roles and responsibilities of each author in the research process. It lists the specific contributions that each author made to the study and manuscript.

Data availability All data generated or analysed during this study are available from the corresponding author on reasonable request.

Declarations

Conflict of interest The authors declare that they have no conflict of interest.

References

1. Sekulić DP, Shah RK. Thermal design theory of three-fluid heat exchangers. Adv Heat Transf. 1995;26:219–328.
2. García-Valladares O. Numerical simulation of triple concentric-tube heat exchangers. Int J Therm Sci. 2004;43:979–91.
3. Sekulić DP. A compact solution of the parallel flow three-fluid heat exchanger problem. Int J Heat Mass Transf. 1994;37:2183–7.
4. Aulds DD, Barron RF. Three-fluid heat exchanger effectiveness. Int J Heat Mass Transf. 1967;10:1457–62.
5. Sekulic DP, Kmecko I. Three-fluid heat exchanger effectiveness—revisited. J Heat Transf. 1995;117:226–9. https://doi.org/10.1115/1.2822309.
6. Saeid NH, Seetharamu KN. Finite element analysis for co-current and counter-current parallel flow three-fluid heat exchanger. Int J Numer Methods Heat Fluid Flow. 2006;16:324–37.
7. Ünal A. Effectiveness-NTU relations for triple concentric-tube heat exchanges. Int Commun Heat Mass Transf. 2003;30:261–72.
8. Ünal A. Theoretical analysis of triple concentric-tube heat exchangers part 2: case studies. Int Commun Heat Mass Transf. 2001;28:243–56.
9. Ünal A. Theoretical analysis of triple concentric-tube heat exchangers part 1: mathematical modelling. Int Commun Heat Mass Transf. 1998;25:949–58.
10. Nema PK, Datta AK. Improved milk fouling simulation in a helical triple tube heat exchanger. Int J Heat Mass Transf. 2006;49:3360–70.
11. Sahoo PK, Ansari IA, Datta AK. Milk fouling simulation in helical triple tube heat exchanger. J Food Eng. 2005;69:235–44.
12. Ghosh I, Sarangi SK, Das PK. Synthesis of multistream heat exchangers by thermally linked two-stream modules. Int J Heat Mass Transf. 2010;53:1070–8.
13. Quadir GA, Badruddin IA, Salman Ahmed NJ. Numerical investigation of the performance of a triple concentric pipe heat exchanger. Int J Heat Mass Transf. 2014;75:165–72.
14. Hashemi Karouei SH, Ajarostaghi SSM, Gorji-Bandpy M, Hosseini Fard SR. Laminar heat transfer and fluid flow of two various hybrid nanofluids in a helical double-pipe heat exchanger equipped with an innovative curved conical turbulator. J Therm Anal Calorim. 2021;143:1455–66. https://doi.org/10.1007/s10973-020-09425-0.

15. Rout A, Singh S, Mohapatra T, Sahoo SS, Solanki CS. Energy, exergy, and economic analysis of an off-grid solar polygeneration system. Energy Convers Manag. 2021;238:114177.
16. Quadir GA, Jarallah SS, Ahmed NJS, Badruddin IA. Experimental investigation of the performance of a triple concentric pipe heat exchanger. Int J Heat Mass Transf. 2013;62:562–6.
17. Radulescu S, Negoita I, (Buchar) IO-RC, 2012 undefined. Heat transfer coefficient solver for a triple concentric-tube heat exchanger in transition regime. Res Radulescu, Negoita, I OnutuRev Chim (Buchar), 2012 esearchgate.net [Internet]. 2016 [cited 2023 Aug 26]; Available from: https://www.researchgate.net/profile/Sinziana-Radulescu/publication/289224033_Heat_Transfer_Coefficient_Solver_for_a_Triple_Concentric-tube_Heat_Exchanger_in_Transition_Regime/links/56be8e6e08ae44da37f8ac36/Heat-Transfer-Coefficient-Solver-for-a-Triple-Co
18. Peigné P, Inard C, Druette L. Experimental study of a triple concentric tube heat exchanger integrated into a wood-based air-heating system for energy-efficient dwellings. Energies. 2013; Available from: https://www.mdpi.com/45316
19. Singh S, Mishra M, Jha PK. Experimental investigations on thermo-hydraulic behaviour of triple concentric-tube heat exchanger. Proc Inst Mech Eng Part E J Process Mech Eng. 1989;229:299–308. https://doi.org/10.1177/0954408914531118.
20. Gomaa A, Halim MA, Elsaid AM. Experimental and numerical investigations of a triple concentric-tube heat exchanger. Appl Therm Eng. 2016;99:1303–15.
21. Gomaa A, Halim MA, Elsaid AM. Enhancement of cooling characteristics and optimization of a triple concentric-tube heat exchanger with inserted ribs. Int J Therm Sci. 2017;120:106–20.
22. Mohapatra T, Padhi BN, Sahoo SS. Experimental investigation of convective heat transfer in an inserted coiled tube type three fluid heat exchanger. Appl Therm Eng. 2017;117:297–307.
23. Touatit A, Bougriou C. Optimal diameters of triple concentric-tube heat exchangers. Int J Heat Technol. 2018;36:367–75.
24. Liang C, Wang Y, Li X. Energy-efficient air conditioning system using a three-fluid heat exchanger for simultaneous temperature and humidity control. Energy Conv Manag; 2022. Available from: https://www.sciencedirect.com/science/article/pii/S0196890422010135
25. Afzal A, Islam MT, Kaladgi AR, Manokar AM, Samuel OD, Mujtaba MA, et al. Experimental investigation on the thermal performance of inserted helical tube three-fluid heat exchanger using graphene/water nanofluid. J Therm Anal Calorim. 2022;147:5087–100.
26. Mohapatra T, Sahoo SS, Mishra SS, Mishra P, Biswal DK. Performance Investigation of a three fluid heat exchanger used in domestic heating applications. Int J Automot Mech Eng. 2022;19:9693–708.
27. Liang C, Wang Y, Li X. Energy-efficient air conditioning system using a three-fluid heat exchanger for simultaneous temperature and humidity control. Energy Convers Manag. 2022;270:116236.
28. Alghamdi KI, Bach CK, Spitler JD, Istiaque F. Modeling, Simulating, and validating a novel three-fluid heat exchanger (Tricoil^{TM}) for a residential heating and air-conditioning system integrating water-based thermal energy storage. [cited 2023 Aug 16]; Available from: https://papers.ssrn.com/abstract=4466045
29. Ruan DF, Yuan XF, Li YR, Wu SY. Entropy generation analysis of parallel and counter-flow three-fluid heat exchangers with three thermal communications. J Non-Equilib Thermodyn. 2011;36:141–54.
30. Panda RC, Sahoo SS, Barik AK, Sahu D, Mohapatra T, Rout A. Performance of solar collector coupled with three fluid heat exchanger and heat storage system for simultaneous water and space heating. Lect Notes Mech Eng. 2023. https://doi.org/10.1007/978-981-19-4388-1_30.
31. Mohapatra T, Ray S, Sahoo SS, Padhi BN. Numerical study on heat transfer and pressure drop characteristics of fluid flow in an inserted coiled tube type three fluid heat exchanger. Heat Transf Res. 2019;48:1440–65. https://doi.org/10.1002/htj.21440.
32. Rogers GFC, Mayhew YR. Heat transfer and pressure loss in helically coiled tubes with turbulent flow. Int J Heat Mass Transf. 1964;7:1207–16.
33. Heat Transfer To Moving Fluids (Journal Article)|OSTI.GOV [Internet]. [cited 2022 Jul 26]. Available from: https://www.osti.gov/biblio/4222485
34. Vicente PG, García A, Viedma A. Experimental investigation on heat transfer and frictional characteristics of spirally corrugated tubes in turbulent flow at different Prandtl numbers. Int J Heat Mass Transf. 2004;47:671–81.
35. Rout A, Sahoo SS, Singh S, Pattnaik S, Barik AK, Awad MM. Benefit-cost analysis and parametric optimization using Taguchi method for a solar water heater. In: Design and performance optimization of renewable energy systems, 2021. p. 101–16.
36. Sahin B, Yakut K, Kotcioglu I, Celik C. Optimum design parameters of a heat exchanger. Appl Energy. 2005;82:90–106.
37. Pandey N, Murugesan K, Thomas HR. Optimization of ground heat exchangers for space heating and cooling applications using Taguchi method and utility concept. Appl Energy. 2017;190:421–38.
38. Miansari M, Valipour MA, Arasteh H, Toghraie D. Energy and exergy analysis and optimization of helically grooved shell and tube heat exchangers by using Taguchi experimental design. J Therm Anal Calorim. 2020;139:3151–64.
39. Mohapatra T, Padhi BN, Sahoo SS. Analytical investigation and performance optimization of a three fluid heat exchanger with helical coil insertion for simultaneous space heating and water heating. Heat Mass Transf Stoffuebertragung. 2019;55:1723–40. https://doi.org/10.1007/s00231-018-02545-2.
40. Chamoli S, Yu P, Kumar A. Multi-response optimization of geometric and flow parameters in a heat exchanger tube with perforated disk inserts by Taguchi grey relational analysis. Appl Therm Eng. 2016;103:1339–50.
41. Celik N, Pusat G, Turgut E. Application of Taguchi method and grey relational analysis on a turbulated heat exchanger. Int J Therm Sci. 2018;124:85–97.
42. Kumar V, Sahoo RR. Parametric and design optimization investigation of a wavy fin and tube air heat exchanger using the T-G technique. Heat Transf. 2022;51:4641–66. https://doi.org/10.1002/htj.22516.